THE JOURNAL OF BIOLOGICAL CHEMISTRY VOL. 281, NO. 29, pp. 20326–20337, July 21, 2006

Resurgent Current and Voltage Sensor Trapping Enhanced Activation by a β-Scorpion Toxin Solely in $Na_v1.6$ Channel

*SIGNIFICANCE IN MICE PURKINJE NEURONS**

Received for publication, January 19, 2006, and in revised form, May 11, 2006 Published, JBC Papers in Press, May 15, 2006, DOI 10.1074/jbc.M600565200

Emanuele Schiavon[‡1,2], Tiziana Sacco[§1], Rita Restano Cassulini[‡2], Georgina Gurrola[¶], Filippo Tempia[§], Lourival D. Possani[¶], and Enzo Wanke[‡¶3]

From the [‡]Department of Biotechnologies and Biosciences, University of Milano-Bicocca, Milan 20126, Italy, the [§]Department of Neurosciences, University of Turin, Turin 10126, Italy, and the [¶]Department of Molecular Medicine and Bioprocesses, Institute of Biotechnology, National Autonomous University of Mexico, Cuernavaca 62271, Morelos, Mexico

Resurgent currents are functionally crucial in sustaining the high frequency firing of cerebellar Purkinje neurons expressing $Na_v1.6$ channels. β-Scorpion toxins, such as CssIV, induce a left shift in the voltage-dependent activation of $Na_v1.2$ channels by "trapping" the IIS4 voltage sensor segment. We found that the dangerous Cn2 β-scorpion peptide induces both the left shift voltage-dependent activation and a transient resurgent current only in human $Na_v1.6$ channels (among 1.1–1.7), whereas CssIV did not induce the resurgent current. Cn2 also produced both actions in mouse Purkinje cells. These findings suggest that only distinct β-toxins produce resurgent currents. We suggest that the novel and unique selectivity of Cn2 could make it a model drug to replace deep brain stimulation of the subthalamic nucleus in patients with Parkinson disease.

Voltage-gated Na^+ channels are responsible for initiating and conducting action potentials in most excitable tissues in vertebrate and invertebrate species. The structural similarity of the seven known tetrodotoxin (TTX)[4]-sensitive α-subunits ($Na_v1.1$–$Na_v1.7$) is relatively high, and biophysical studies of the effects of specific toxins have been crucial for extending our understanding of the structure and function of ion channels (1, 2). The S3–S4 extracellular loops of domains II and IV have been identified as the targets of β- and α-scorpion toxins (and sea anemone toxins), respectively (3–6). Specifically, studies have demonstrated that the β-scorpion toxin CssIV interacts strongly with the IIS3-S4 loop. By binding to the extracellular end of the IIS4 voltage sensor segment, the toxin stabilizes and traps it in the outward (activated) position, enhancing the probability of channel opening and, thus, producing the negative shift in the voltage dependence of activation (the voltage sensor-trapping model; see Ref. 4). To some extent, these studies explained previous observations of scorpion venom actions (7) and the effects of β-scorpion toxins on frog and toad Ranvier nodes (8, 9). In contrast, sea anemone toxins and α-scorpion toxins disrupt the inactivation process by interacting with the extracellular IVS3-S4 loop (3).

The resurgent current has been defined as an unexpected behavior exhibited by an inactivated channel that "conventionally" should not be able to reopen immediately upon repolarization at potentials where it normally opens (10). Discovered in dissociated cerebellar Purkinje neurons, a working model assumes, at the channel cytoplasmic face, the existence of an intrinsic blocking particle (not conventional) functioning in parallel with the inactivation particle (conventional) in a mutually exclusive way. During strong, brief depolarizations, the blocking particle obstructs open Na^+ channels, producing the "unconventional" inactivated state. Repolarization expels the blocking particle from the inner mouth of the open channel, initiating a phase of resurgent current that terminates with classical inactivation (10–12).

We studied the biophysical effects of Cn2 toxin (13) purified from the venom of the Mexican scorpion *Centruroides noxius* on various human Na^+ channel isoforms ($Na_v1.1$–$Na_v1.7$). We discovered that Cn2 is only capable of inducing the voltage sensor-trapping mechanism in the $hNa_v1.6$ channel current recorded in stably transfected HEK cells and in wild-type cerebellar Purkinje cells. Moreover, we found that Cn2 generates a novel transient resurgent current in both cell types (11).

EXPERIMENTAL PROCEDURES

Toxin Purification and Molecular Modeling

Cn2 was purified from the venom of the scorpion *C. noxius* using a previously described technique (14). CssIV (15) was purified from the venom of the scorpion *Centruroides suffusus suffusus* using a procedure modified from Martin *et al.* (16). We collected the scorpions in the field and then extracted and separated the venom using high performance liquid chromatography (HPLC). Briefly, the soluble venom was fractionated by HPLC using a C18 reverse-phase column in the presence of

* This study was supported in part by Italian Ministero dell'Università e della Ricerca Scientifica e Tecnologica Grants MIUR-PRIN2003-2005-2001055320 and 2003052919, MIUR-FIRB2001-RBNE01XMP4-002, and MIUR-FISR2001 0300179 and the Università di Milano-Bicocca (to E. W.). It also was supported by the National Council of Science and Technology (Mexican Government Grant 40251-Q) and by Direción General de Asuntos de Personal Académico Grant IN206003 of the National Autonomous University of Mexico (to L. D. P.). The costs of publication of this article were defrayed in part by the payment of page charges. This article must therefore be hereby marked "*advertisement*" in accordance with 18 U.S.C. Section 1734 solely to indicate this fact.

[1] These two authors contributed equally to this work.

[2] Ph.D. student of Physiology at the Department of Biotechnologies and Biosciences of the University of Milano-Bicocca.

[3] To whom correspondence should be addressed: Dipartimento di Biotecnologie e Bioscience, Università di Milano-Bicocca, Piazza della Scienza, 2U3, 20126 Milan, Italy. E-mail: enzo.wanke@unimib.it.

[4] The abbreviations used are: TTX, tetrodotoxin; HPLC, high pressure liquid chromatography; VC, voltage clamp.

0.1% trifluoroacetic acid and then eluted using a linear gradient of 0–60% acetonitrile. The component with the expected molecular mass determined by means of mass spectrometry (Finigan LCQ^{DUO} electrospray) was further purified by two additional steps.[5] CssIV elutes at 27.1 min in a gradient of 20–60% acetonitrile in 0.1% trifluoroacetic acid. The theoretical molecular mass (7602.6 atomic mass units) and that measured experimentally (7602.0 atomic mass units) were as expected from the previously established primary structure (Swiss Protein accession number P60266). Additionally, the first 17 amino acid residues in the N-terminal region of CssIV were directly determined on the basis of automatic Edman degradation (LF 3000 Protein Sequencer; Beckman) in order to confirm the sequence. The CssIV sequence underwent homology modeling using the SWISS-MODEL server (17) and the lowest energy conformer in the Protein Data Bank entry 1Cn2 as template (13). After a second round of refinement, the quality of the final model is equivalent to that of the template (assessed by the WHAT_CHECK program (18)), so no further (on-bench) refinement was used. The three-dimensional structure of Cn2 and the model of CssIV were visualized using the MOLMOL program (19).

Electrophysiology

Cell Culture—HEK293 cell lines stably expressing human $Na_v1.1$, −1.2, −1.3, −1.5, and −1.6 (generously donated by Dr. J. J. Clare of GlaxoSmithKline, Stevenage, UK) were cultured in modified Dulbecco's medium supplemented with 10% fetal bovine serum as described by Olivera *et al.* (20). $Na_v1.4$-expressing cells were obtained by stably transfecting a plasmid containing the $hNa_v1.4$ construct (a kind gift from Prof. Diana Conti-Camerino, University of Bari, Italy). In order to test the $Na_v1.7$ channels, we used primary cultures of rat chromaffin cells (see Ref. 21 for details), since the selective presence of this channel alone is well documented (22) (see Ref. 23 for a review).

Solutions and Drugs—The standard extracellular solution contained 130 mM NaCl, 5 mM KCl, 2 mM $CaCl_2$, 2 mM $MgCl_2$, 10 mM HEPES-NaOH, 5 mM D-glucose, pH 7.40. The standard pipette solution contained 130 mM K^+-aspartate, 10 mM NaCl, 2 mM $MgCl_2$, 10 mM EGTA-KOH, 10 mM Hepes-KOH, pH 7.30. About 6–8% of the cells in the clone expressing $Na_v1.6$ channels had a persistent Na^+ current, as reported by Burbidge *et al.* (24). We systematically tested these cells and discarded those showing incomplete inactivation (a residual current after 250 ms of <0.1% of the peak Na^+ current). Known quantities of the toxins were dissolved in the extracellular solution immediately before the experiments. TTX (Sigma) was used at 100 nM on the $Na_v1.1$, -1.2, -1.3, -1.4, -1.6, and -1.7 currents, and the resulting traces were subtracted from the control traces to obtain the TTX-sensitive currents; the $Na_v1.5$ clone (which has a much higher TTX ID_{50} than 100 nM) never showed any significant potassium currents at the test potentials (25). The extracellular solutions were delivered through a remote-controlled 9-hole (0.6 mm) linear positioner placed near the cell under study, and the average response time was 2–3 s.

Patch Clamp Recordings and Data Analysis—The currents were recorded at room temperature using the MultiClamp 700A (Axon Instruments) as previously described (21); pipette resistance was about 1.3–2.1 megaohms; cell capacitance and series resistance errors were carefully (85–90%) compensated for before each run of the voltage clamp protocol in order to reduce voltage errors to less than 5% of the protocol pulse. The P/N leak procedure was routinely used. pClamp 8.2 (Axon Instruments) and Origin 7 (Microcal Inc.) software were routinely used during data acquisition and analysis. All of the data regarding inactivation (see Figs. 1*D* and 2, *C* and *D*) were obtained using the following protocols. 1) For development, from a holding potential of −120 mV, the cells were prepulsed to the conditioning voltage (−70, −60, −50 mV) and then stepped to −10 mV to determine the fraction of current inactivated during the prepulse at 1, 2, 5, 10, 20, 50, 100, 200, 500, 1000 ms. 2) For recovery, the cells were pulsed at −10 mV for 40 ms and conditioned at the same potentials as before and then stepped again to −10 mV to determine the fraction of current recovered during the prepulse at 1, 2, 5, 10, 20, 50, 100, 250 ms.

Electrophysiology in Purkinje Cells—Whole-cell Na^+ currents and membrane voltage were recorded from Purkinje neurons in cerebellar slices prepared from 4–7-day-old mice for voltage clamp (VC) recordings and 23–38-day-old mice for current clamp. Mice of the CD1 strain were used to characterize the effects of Cn2 on sodium currents and action potential discharge of Purkinje cells. Parasagittal cerebellar slices (300-μm thickness) were obtained following a previously described technique (26, 27), kept for 1 h at 35 °C and then at room temperature in the extracellular saline solution containing 125 mM NaCl, 2.5 mM KCl, 2 mM $CaCl_2$, 1 mM $MgCl_2$, 1.25 mM NaH_2PO_4, 26 mM $NaHCO_3$, 20 mM glucose, bubbled with 95% O_2, 5% CO_2 (pH 7.4). The recording chamber was continuously perfused at room temperature (about 22 °C) with the bubbled saline solution at a rate of 2.5 ml/min. The Purkinje neuron upper surface was cleaned by a sodalime glass pipette filled with the extracellular saline solution. Membrane currents or voltage were recorded by an EPC-9C patch clamp amplifier (HEKA Elektronik, Lambrecht/Pfalz, Germany), filtered at 8.6 kHz, and digitized at 20 kHz. Digitized data were stored on a Macintosh computer (G3, Apple Computer, Cupertino, CA) using the Pulse software (HEKA Elektronik, Lambrecht/Pfalz, Germany) and analyzed by the Igor Pro software (Wavemetrics, Lake Oswego, OR). For VC recordings, patch pipettes (2.5–3.0 megaohms) were filled with the following solution: 112 mM CsCl, 9 mM HEPES, 9 mM EGTA, 4 mM $MgCl_2$, 14 mM phosphocreatine di(tris) salt, 4 mM Na_2ATP, 0.4 mM Na_3GTP. The external saline solution contained 40 mM NaCl, 113 mM TEA-Cl, 10 mM HEPES, 2 mM $BaCl_2$, 0.3 mM $CdCl_2$, pH 7.4. In VC, the uncompensated value of series resistance was 4–8 megaohms, and series resistance compensation was set at 90%. For the young Purkinje neurons used for VC recordings, in these conditions, space clamp problems are minimal or absent even for the most distal cellular compartments (27). The cell was kept at a holding potential of −70 mV. In current clamp recordings, the internal solution contained 140 mM potassium gluconate, 10 mM HEPES, 0.5 mM EGTA, 4 mM $MgCl_2$, 4 mM Na_2ATP, 0.4 mM Na_3GTP. The external solution was the extracellular saline

[5] G. Corzo, E. Wanke, and L. D. Possani, manuscript in preparation.

used for slice preparation and maintenance. Both in VC and current clamp experiments, $GABA_A$ and ionotropic glutamate receptors were kept blocked by bicuculline methochloride (20 μM) and kynurenic acid (1 mM). All solutions and drugs were applied by changing the perfusion line, except the Cn2 toxin, which was directly added to the recording chamber at 140 nM. The concentration of Cn2 in the chamber was calculated from the amount added and the final volume of solution. The final concentration of Cn2 applied to CD1 mice was always between 35 and 40 nM. The effect of the Cn2 toxin began immediately but increased for a few minutes, during which it diffused inside the tissue. In order to follow the wash-in of Cn2 action, the stimulation protocol was applied every minute. The effect of Cn2 saturated within 5 min. At the end of each VC recording session, the Na^+ channel blocker TTX (0.5 μM) was applied. The traces in TTX were used to subtract capacitive and leak currents. Salts were purchased from Sigma, and TTX and receptor blockers were from Tocris Cookson (Langford, UK).

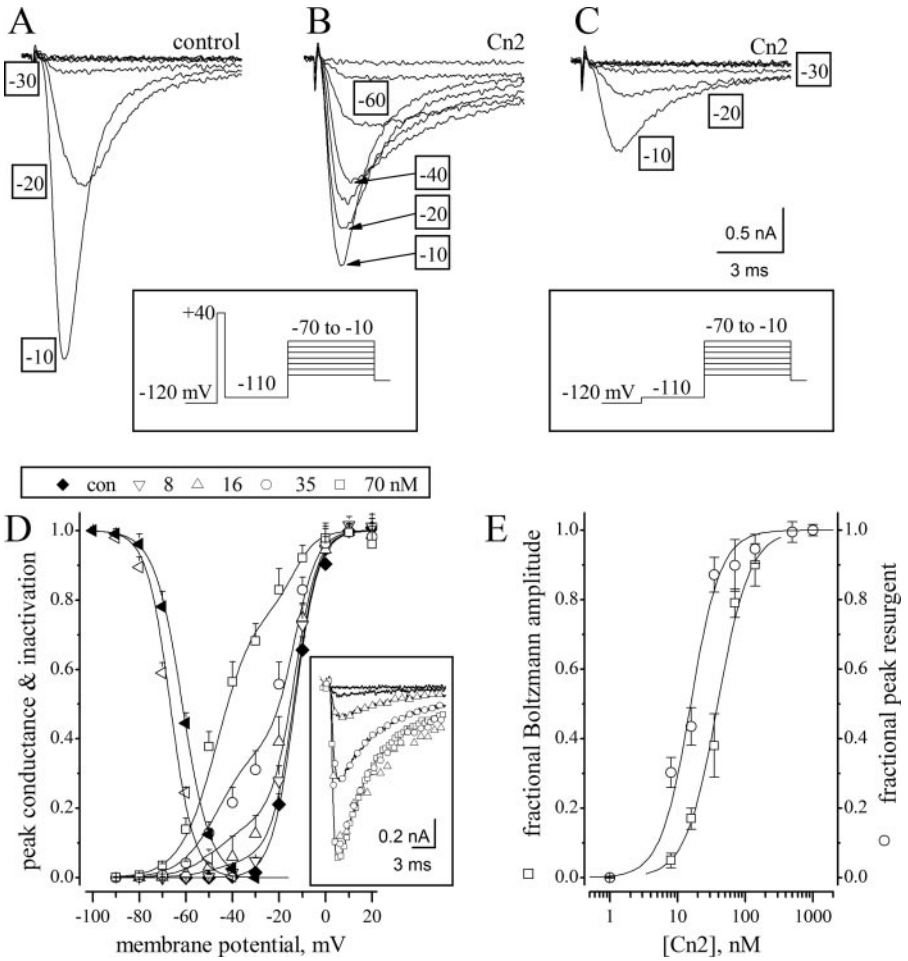

FIGURE 1. **Cn2 is a potent β-scorpion toxin for $Na_v1.6$ channels.** *A–C*, superimposed traces of Na^+ currents elicited, in a $Na_v1.6$-expressing cell, by using the protocols shown in the *lower insets* in control (*A*) and with 140 nM Cn2 (*B* and *C*). *D*, on the *right part* of the plot, normalized peak conductance-voltage plot at different Cn2 concentrations (8 nM ▽, 16 nM △, 35 nM ○, and 70 nM □; $n = 4$); normalization factors were 1, 1.07, 1.26 and 1.83, respectively. The *solid lines* through the data are fits to a sum of two Boltzmann relationships whose amplitudes sum is 1, one corresponding to the normal channels and the other corresponding to those that were bound by the toxin. The voltage dependence of the control data (◆) were found assuming a 0 value for the amplitude of one Boltzmann curve, and the $V_{1/2}$ (−13.2 ± 0.4 mV) and slope (5 ± 0.3 mV) were maintained fixed during fitting of the other data at various Cn2 concentrations. By using the 70 nM concentration data, we found, for the other Boltzmann curve, novel values of $V_{1/2}$ (−46.4 ± 2.1), slope (7.98 ± 1.9), and amplitude (0.79 ± 0.1). For the other concentrations (35, 16, and 8 nM), we maintained fixed all parameters except the amplitude of the Cn2-shifted activation curve, and the amplitudes that resulted were 0.38 ± 0.1, 0.16 ± 0.02, and 0.05 ± 0.01, respectively. *Left part* of the *plot*, the inactivation in control (◀) and during a 140 nM Cn2 action (◁) derived from the development of inactivation data (not shown; $n = 5$). The *lines through symbols* are Boltzmann functions with the following $V_{1/2}$ and slope: −61.3 ± 0.3 and 6 ± 0.3 in control and −65.3 ± 0.4 and 6.3 ± 0.2 in Cn2 (140 nM, $n = 4$). *Inset*, superimposed traces of currents from a single cell, elicited at −40 mV at the indicated concentrations. *Symbols* and *lines* are as follows. *Lines*, control and 8 nM Cn2; *lines* with the *same symbols* as in *D*, 16, 35, and 70 nM Cn2; *symbols*, the 16 and 35 nM data normalized to the 70 nM amplitude. *E*, dose-response relationship obtained by plotting the amplitudes of the left-shifted Boltzmann curves as shown in *D* (□, *left y-axis*) and the fractional peak resurgent currents (○, *right y-axis*) (see below; $n = 6$). Fitting of Boltzmann amplitude and resurgent current to Hill curves (*continuous lines*) resulted in the following values of EC_{50} and Hill coefficient: 39.2 ± 3.7 and 15.5 ± 2.3 nM and 1.82 ± 0.2 and 1.97 ± 0.3, respectively.

RESULTS

Cn2 Is a β-Scorpion Toxin Only for $Na_v1.6$ Channels—Since Cn2 doses of up to 0.3 μM had no effect on the cells expressing $Na_v1.1$, $Na_v1.2$, $Na_v1.3$, $Na_v1.4$, $Na_v1.5$, and $Na_v1.7$ α-subunits (see below; Fig. 4), we present here data obtained using HEK cells stably expressing the human α-subunit of $Na_v1.6$ channels (20). Previous experiments using *Xenopus* oocytes transiently expressing $Na_v1.6$ channels with or without β-subunits (28) have shown the presence of small persistent currents.

The effect of Cn2 toxin on $Na_v1.6$-expressing cells is dose-dependent and looks like that of CssIV described in $rNa_v1.2$ (4, 6). The classical prepulse conditioned protocol (7) (see *insets* to Fig. 1, *A* and *B*) used to induce the left shift of the activation curve modified the channel biophysics in a manner that can be readily interpreted in the framework of the negative shift of the voltage-dependent activation. In Fig. 1, *A–C*, are shown the Na^+ current recordings with or without a brief prepulse to +40 mV in control and in the presence of 140 nM of toxin. The current has a threshold of about −30 mV under control conditions (with or without prepulse), but toxin perfusion shifted it negatively to −60 mV. The peak inward currents were depressed 10–15%, depending on the toxin concentration and perfusion time. However, without the prepulse, a strong blocking action (see Fig. 1*C*) reproduced the properties of typical β-scorpion toxins. Both effects were recorded simultaneously, unlike the immediate left shift to −60 mV and delayed blocking at 0 mV caused by CssIV in $rNa_v1.2$ (4).

Fig. 1*D* shows the effects of different Cn2 concentrations (8–70 nM) on normalized voltage-dependent conductances.

Assuming that the channels exist in two forms (6, 7), with and without toxin, the data were fitted by the sum of two Boltzmann relationships with concentration-dependent amplitudes (see legend of Fig. 1*D*). The *inset* of Fig. 1*D* (experiment in the same cell) shows that the currents elicited at −40 mV during the concentration increase are superimposable (see *different symbols* superimposed on the 70 nM data). These data demonstrate that the toxin and prepulse are responsible for revealing and facilitating the appearance of currents normally unavailable at more hyperpolarized membrane potentials, through the negative shift of the activation curve.

By plotting in Fig. 1*E* (*left axis*), the concentration-dependent fractional increase in the amplitude of the left-shifted Boltzmann curve, which represents the proportion of the channels to which Cn2 was attached ($n = 4$), we could predict the EC_{50} of this process as being 39.2 ± 3.7 nM with a Hill coefficient of 1.82 ± 0.2, a value that suggests more than one binding site.

Prepulse- and Cn2-induced Currents in the Region from −70 to −40 mV Disappear after 300 ms—In the region positive to −35 mV (threshold of activation in control), the time course of the currents in the presence of Cn2 was not significantly different from control (not shown). In contrast, a comparison between control and Cn2 was impossible in the novel region from −75 to −35 mV, because no currents can be elicited in control conditions. Nevertheless, we asked how the Cn2-induced currents at potentials below the control threshold could depend on the delay between the prepulse and the test potential. In other words, following the framework of the voltage sensor-trapping model (4), we tested the possibility that the peptide toxin, after binding the outwardly moved S4 segments during the prepulse (so-called "primed channel"), could eventually unbind from the channel protein.

In order to study the properties of the currents elicited by the 10-ms prepulse to +30 mV, we introduced a variable duration (from 2.5 to 200 ms at −100 mV) between the prepulse and the test pulse (see protocol in Fig. 2*A*). As shown in Fig. 2*A* (where the test potential was −50 mV), these experiments revealed that 1) all of currents turn on with very fast kinetics (time to peak ~1 ms), 2) the traces finally overlap on a slowly decaying component, and 3) the first part of each decaying trace has a faster decaying component. Fitting to a double exponential decaying function showed that the very slow decaying component is neither voltage-dependent nor toxin concentration-dependent but characterized by a time constant of about 104.2 ± 5.7 ms ($n = 5$). On the contrary, the fast inactivation component had voltage-dependent time constants: 9.5 ± 1.1 ms at −50 mV and 13.5 ± 1.4 ms at −60 mV ($n = 5$).

In Fig. 2*B*, we plotted the fractional amplitudes of the slow (□) and fast (○) components at −50 and −60 mV (averaged) against the duration of the −100 mV level. The slow component resulted in a decaying process with a time constant of 104 ± 6.2 ms ($n = 4$). The fast component reached its maximum in about ~10 ms but then matched the slow component decaying process. The ratio between the fast component and total peak was higher at −50 (△) than at −60 mV (▲) and time-independent, suggesting a common underlying progression.

Collectively, these data suggest that the negative shift of the voltage-dependent activation, induced by the combined actions of toxin and prepulse, is not a steady-state process but instead a transient machinery that disappears with a time constant of ~100 ms. Similar effects and hypotheses have been reported with scorpion venoms (7).

Channels inactivated by a strong prepulse to +30 have enough time to quickly transition from an inactivated state to a closed state when stepped to −100 for at least 5–10 ms. From the closed state, channels are able to rapidly reopen at −60 mV, thus following the conventional recovery from inactivation. If this time is reduced to zero, conventional recovery should suggest no available current. Surprisingly, we recorded a new current shown in Fig. 2*A* at −50 (*circles*) and −60 mV (*triangles*) that is characterized by two phases, a moderately fast increase with a peak at about 20 ms and a much slower decay that mimics the 100-ms decay previously observed and characterized.

To investigate if Cn2 also affected the voltage-dependent inactivation mechanisms, we compared development and recovery of inactivation. From development of inactivation protocols (see "Experimental Procedures"), we obtained the data shown in Fig. 1*D* (*left axis*, ◀, control; ◁, Cn2). In Cn2, the best fitted Boltzmann curves negatively shifted by about 4–5 mV; however, the data were not statistically significant (see legend to Fig. 1).

Recovery from inactivation was obtained by using the double pulse protocol (see "Experimental Procedures"). In control, at conditioning of −70 mV (see Fig. 2*C*, *top*), the envelope of the peaks was monotonic, and a similar exponential time course was observed also at −60 and −50 mV with time constants τ_{rec} (V_m), of 17.7 ± 1.4, 26.9 ± 1.5, and 25.7 ± 2.2 ms, respectively ($n = 5$). All of these control time constants agree with similar data reported for the $rNa_v1.6$ channel (29).

However, in Cn2 (Fig. 2*C*, bottom), when potential was suddenly stepped from −10 to −70 mV, a novel current started to increase until the test pulse was stepped again to −10 mV. With long preconditioning durations at −70 mV, the time course of the novel current resembled the time course already seen in Fig. 2*A* (*symbols*). With preconditionings at −60 and −50 mV, results were very similar (not shown). The analyses of all of these data are plotted in Fig. 2*D* for control experiments (*left scale*, *closed symbols*) and for Cn2 (*right scale*, *open symbols*). The Cn2 data indicate, in the recovery from inactivation, a peak at about 23 ms ($n = 6$). This value approximately corresponds to the time to peak of the novel current and a decaying time course similar to that seen in Fig. 2*B*.

Properties of Cn2-induced Resurgent Currents in $Na_v1.6$ Channels: Voltage Dependence and the Boosting Effect of ATX-II—The currents observed in the region from −70 to −40 mV, induced by strong depolarizations, previously shown in Fig. 2, *A* (*symbols*), *C*, and *D*, resemble the so-called venom-induced current (*Centruroides sculpturatus*) observed by Cahalan (7) in the frog Ranvier node. Such currents have been interpreted and modeled as recovery from the inactivation process. Indeed, the time constants of the exponentially increasing venom-induced current were not different from the corresponding time constants of the recovery from inactivation. However, subsequent experiments (9) conducted with purified peptides from the

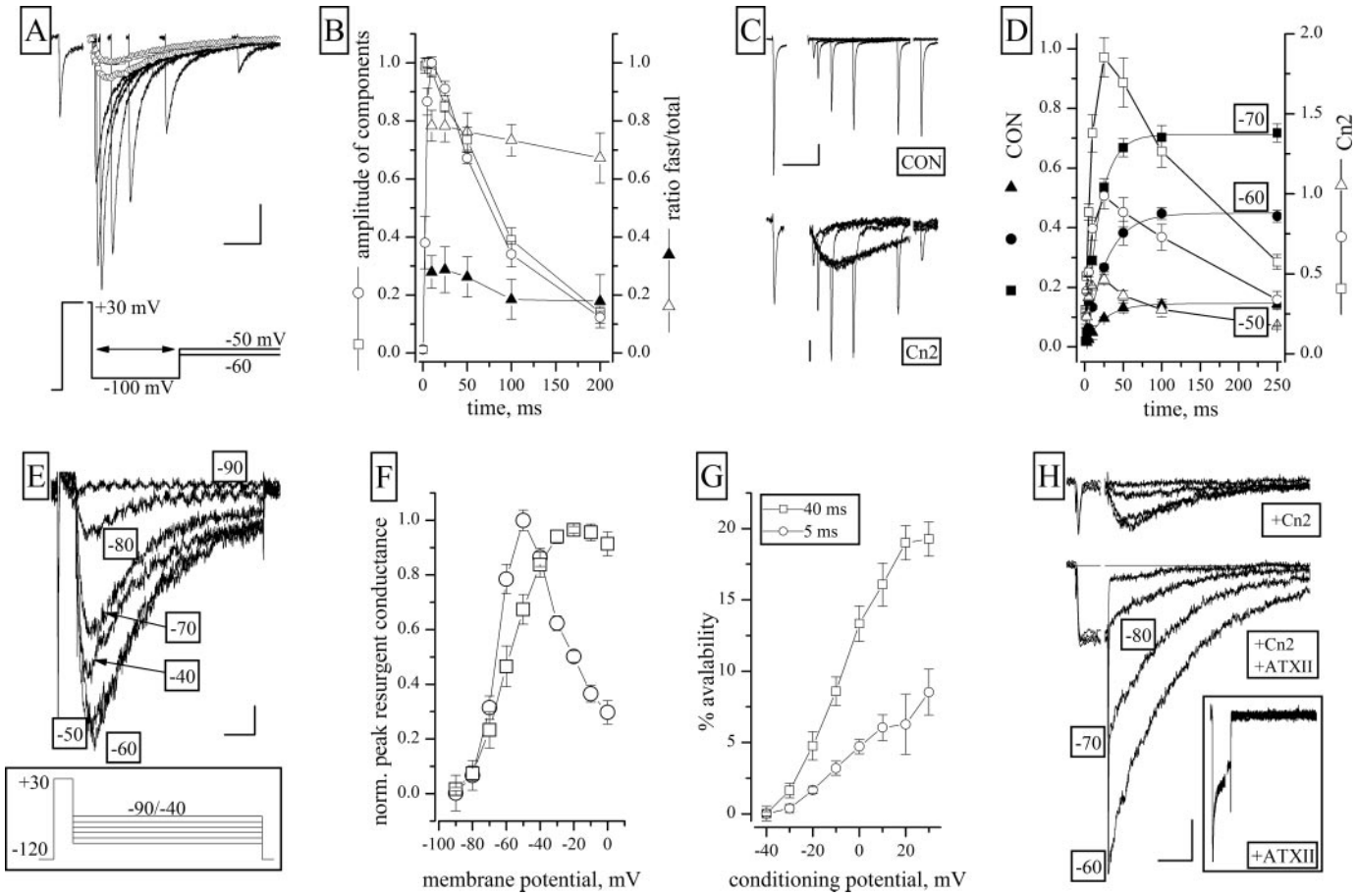

FIGURE 2. **Properties of Cn2-induced currents decay and of the Cn2-induced resurgent currents.** *A*, family of currents (*lines*) induced by Cn2 at −50 mV according to the protocol shown below. Currents elicited without any repolarization to −100 mV are shown in *symbols* at −50 (*open circles*) and −60 mV (*open triangles*). *Scale bars*, 1 nA/50 ms. *B*, plot of the fractional amplitudes of the slow (□) and (○) fast components obtained after fitting the decaying part of the traces shown in *A* (see "Results"). The ratio of the fast component to total is plotted at −50 (△) and −60 (▲) mV. *C*, experiments for studying recovery from inactivation in control (*top*) and in Cn2 (*bottom*) in the same cell. Shown are superimposed traces of Na^+ currents elicited at −10 mV but after preconditionings at −70 mV for different times. *Scale bars*, 1 nA/40 ms (*top*) and 0.2 nA (*bottom*). *D*, plot of the fractional recovery from inactivation, at different potentials, in control (*left y-axis*, *closed symbols*) and in Cn2 (*right y-axis*, only at −70 mV, *open symbols*). The *continuous line* through the *closed points* (control) are exponentials with τ_{rec} (V_m) time constants reported under "Results." *E*, superimposed traces of Na^+ currents elicited, in an $Na_v1.6$-expressing cell, by using the protocols shown in the *inset*. A concentration of 140 nM Cn2 was used. *Scale bars*, 100 pA/40 ms. *F*, normalized peak conductance-voltage plot of the resurgent current (data (○) obtained from cells at different Cn2 concentrations (from 15 to 150 nM, $n = 5$)). Data shown with a *symbol* □ represent the average of five experiments described in *E* (see below). *G*, percentage availability, calculated as peak resurgent current (at −60 mV) normalized by the maximal peak current previously elicited by 5-ms-long (□) or 40-ms-long (○) pulses. A concentration of 140 nM Cn2 was used. *H*, *upper* and *lower parts* show resurgent currents (at 70 nM, Cn2), elicited in the −90/−60 interval from +30 mV, without or with 300 nM ATX-II (same cell and same scales). *Scale bars*, 300 pA/50 ms. *Inset*, currents from a cell, in the presence of ATX-II, in which the same protocols were used but the test pulse was from −90 to −40 mV. Notice the absence of inward currents.

same scorpion on *Bufo marinus* and *Rana pipiens* nodes did not match the previous results of the Cahalan (7) paper. Moreover, venom-induced currents also resemble those observed in Purkinje cells, namely resurgent currents (10, 30). A key point is that the density of $Na_v1.6$ channels should be very high in both the node and Purkinje cells (31, 32).

Following the classic protocol that recovers Na^+ channels after complete inactivation, we depolarized the cell to +30 mV for 25 ms and immediately tested the current in the −90 to −40 mV range (see *inset* to Fig. 2*E*). The results (shown in Fig. 2*E*) are very similar to those obtained by Raman and Bean in Purkinje cells (10). Starting from −80 mV, a resurgent current slowly rises and then very slowly decays. In the region from −80 to −30 mV, we fit the rising phase with an exponential function. The corresponding time constants τ_{Cn2} in ms were as follows (V_m in parenthesis): 4.5 ± 0.9 (−80), 6.3 ± 1.2 (−70), 7.3 ± 0.6 (−60), 7.1 ± 0.5 (−50), 4.4 ± 0.4 (−40), 3.7 ± 0.6 (−30) ($n = 5$). These values are all about three times smaller than the τ_{rec} (V_m) at the same membrane potentials, suggesting a mechanism much faster than that conventionally operating in control and, thus, different from that previously hypothesized for the scorpion venom, which is known to be a mixture of many peptides (7).

By means of experiments like those shown in Fig. 2*E*, it was possible to calculate a normalized peak resurgent conductance G-V plot (Fig. 2*F*). The plot was independent of Cn2 concentrations (Fig. 2*F*, ○, from 70 to 140 nM), and the peak of the bell-shaped curve was always observed at about −55 mV. This value is 20 mV more negative than the value observed for the intrinsic resurgent current in Purkinje cells (10) and about 15 mV more positive than the venom-induced current observed in the frog node (7). As shown in Fig. 2*G*, increasing or reducing the duration and the voltage of the predepolarization made it possible to obtain more or less resurgent currents. The percent-

age availability of channels producing the resurgent component increased as a function of membrane potential and duration; 40-ms depolarizing pulses saturated the availability, which reached about 20% of the peak current ($n = 3$).

This result is different from the reported dependence of resurgent currents in the cerebellum (30) and could suggest that more time is necessary to increase the probability of the toxin finding the best channel conformation for binding.

Similar recordings of resurgent current can be obtained also if the sodium channels never opened, because they were slowly inactivated from closed states (not shown). This suggests that regardless of the route followed by channels during the open/inactivated states, a strong positive membrane potential is crucial to the production of I_{NaR}.

In an attempt to explain the bell-shaped voltage-dependent resurgent conductance shown in Fig. 2*F*, we used ATX-II, a classical toxin that potently slows fast inactivation (3, 20). The *upper* and *lower parts* of Fig. 2*H* show I_{NaR} recordings without and with the addition of 300 nM ATX-II. The recordings were obtained from the same cell, and the graphs are shown at the same scale and test potentials (−90, −80, −70, and −60 mV) in order to highlight the potentiating effect of ATX-II. Unlike the experiments using Cn2 alone, the addition of ATX-II produced currents characterized by a single decaying current whose time course can be fitted with a time constant (95.7 ± 7.2 ms, $n = 5$) similar to that characterizing the disappearance of the β-toxin left shift shown in Fig. 2*A* (*top*). The traces shown in the *inset*, elicited using the same command protocol, were obtained in another cell perfused with ATX-II alone in order to verify that this toxin does not affect the properties of the machinery responsible for I_{NaR} mechanisms in the voltage range from −90 to −40 mV. On the basis of results from five additional experiments in which Cn2 and ATX-II were applied consecutively in different order, we plotted the average peak resurgent conductance (Fig. 2*F*, □). These data clearly show that the decreasing right part (positive to −50 mV) of the voltage-dependent Cn2-induced resurgent conductance (Fig. 2*F*, ○) is due to the fast inactivation of the primed channels.

Furthermore, I_{NaR} experiments ($n = 6$) using different Cn2 concentrations led to the normalized peak I_{NaR} data shown in the *right axis* of Fig. 1*E*. After fitting these data to a Hill curve, the EC_{50} and Hill coefficient were 15.5 ± 2.3 and 1.97 ± 0.3 nM, respectively, suggesting that the Cn2 peptide exerts these effects with higher affinity than that observed for the left shift displacement of voltage-dependent activation.

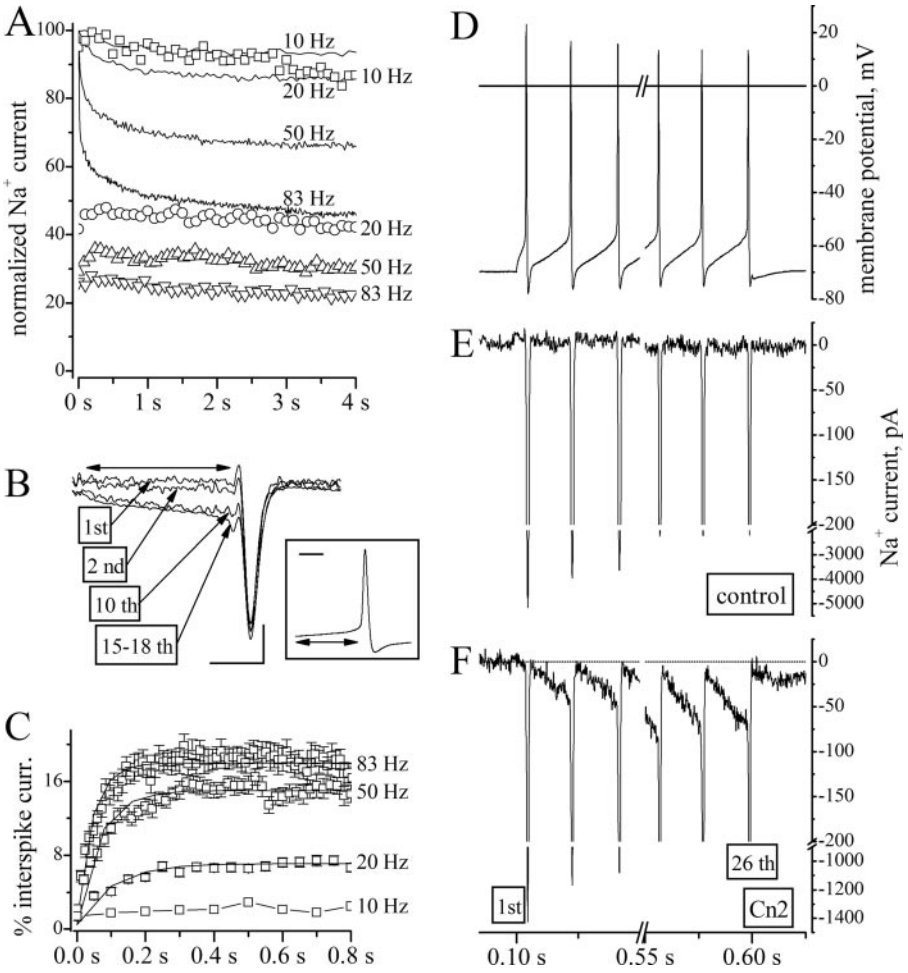

FIGURE 3. **Action potential clamp of $Na_v1.6$ cells with Purkinje action potentials.** *A*, plot of the normalized peak Na^+ current obtained in a $Na_v1.6$ cell voltage-clamped with trains of Purkinje action potentials (see *inset* to *B*; holding potential −65 mV) at the indicated frequencies in control (*lines*) and in 140 nM Cn2 (*symbols*; the high frequency data are decimated). Data in Cn2 were multiplied by a factor 3.9 to compensate for the blocking effect of the toxin. *B*, superimposed traces of the TTX-sensitive currents obtained during the action potential clamp experiments (83 Hz). *Traces* corresponding to the first, second, and 10th experiments and the average of *traces 15–18* are shown as indicated. *Scale bars*, 300 pA and 2 ms. *Inset*, the action potential used to elicit the currents. *Scale bar*, 3 ms. *C*, plot of the percentage average interspike current during the time interval shown by the *horizontal arrow* in *C* (interspike interval), during the trains at the indicated frequencies. The *continuous lines* are exponentials, with time constants of 43 ± 4.2, 64 ± 5.1, and 100 ± 6.2 ms ($n = 3$), fitted on the experimental points from experiments at 83, 50, and 20 Hz, respectively. *D*, recording of a 0.5-s 26-spike train of action potentials from a Purkinje cell. (Note that the *x scale* has a *break* as in *F*). *E* and *F*, action potential clamp recordings of the TTX-sensitive currents using the *trace* shown in *D*, in control (*E*) and in Cn2 (*F*). Note that the *x*- and *y-scales* have a *break*.

In the Presence of Cn2, Brief Firing Is Enough to Provoke Resurgent Current Accumulation—In order to ascertain the action of Cn2 toxin under physiological conditions, we voltage-clamped cells expressing $Na_v1.6$ channels using protocols obtained by summing rat Purkinje cell action potentials at frequencies of 83, 50, 20, and 10 Hz. In Fig. 3*A*, the time course of the peak TTX-sensitive currents are shown under control conditions (*lines*) and during Cn2 perfusion (*symbols*). The application of Cn2 (140 nM) depressed peak current availability by a factor of 3.9. Whereas the decaying curves observed in control

reproduced the effects of fast and slow inactivation with a maximal depression of about 50% at 83 Hz, in contrast, the Cn2 traces are almost constant.

It should be remembered that in these experiments the action potential takes the place of the priming pulse in the experiments previously illustrated in Figs. 1 and 2. The superimposed currents induced by Cn2 at 83 Hz are shown in Fig. 3*B*. Detailed inspection of the Na^+ traces between the spikes (see *horizontal double arrow line*) revealed an enhanced averaged current from the first up to about the 20th spike. Complete analyses of these data at 83, 50, 20, and 10 Hz are shown in Fig. 3*C*. Fitting of the data indicated that this is an exponential process with different time constants at different spike train frequencies (see legend to Fig. 3), and it is worth noting that the availability of this resurgent current is greatest at high frequency, whereas that of the peak current is greatest at low frequency (Fig. 3*A*). Finally, voltage clamping the cells with a single Purkinje train (~50 Hz; Fig. 3*D*) showed that there was an accumulation of the interspike current in the Cn2-treated cells (Fig. 3*F*) but not in the control (Fig. 3*E*).

On the whole, we suggest that the time course of the resurgent current and its transient properties illustrated in Fig. 2, *E–H*, is entirely compatible with the boosting of the current availability when the interspike duration decreases from 100 to 12 ms.

Cn2 and CssIV β-Scorpion Toxins Differently Affect the Sodium Channel Isoforms—To complete our analysis, we compared the effects of Cn2 with another β-scorpion toxin CssIV on additional Na^+ channel isoforms. Fig. 4 summarizes the results of experiments conducted using 300 nM CssIV (see *grid columns*) compared with those performed using Cn2 (*black columns*) at the same concentration (except in $Na_v1.6$; *black columns* with *open circle*). To evaluate the negative shift action of the peptides, we tested the seven Na^+ channel isoforms under primed or unprimed conditions. The data, shown on the *right z-axis*, are expressed as the peak fractional current tested at a membrane potential 10 mV more negative than the control threshold. The fractional peak resurgent current is plotted on the *left z-axis*. The results indicate that Cn2 is highly selective for the $Na_v1.6$ isoform and produces a resurgent current, whereas CssIV is less selective and is unable to produce a resurgent current.

We investigated whether CssIV produces a shift of activation that is time-dependent as shown for Cn2 in Fig. 2, *A* and *B*. These experiments were performed using isoforms $Na_v1.1$, $Na_v1.2$, and $Na_v1.6$. The results show that dissociation at −100 mV is characterized in $Na_v1.1$ by a time constant of 0.45 ± 0.04 s ($n = 3$), which is approximately 5 times larger than that observed for Cn2. Experiments with isoforms $Na_v1.2$ and $Na_v1.6$ were characterized by two time constants of approximately equal contribution, with the following values ($n = 3$); in $Na_v1.2$, τ_f was 0.035 ± 0.01, and τ_s was 0.9 ± 0.15 s; in $Na_v1.6$, τ_f was 0.062 ± 0.015, and τ_s was 1.4 ± 0.31 s.

These data show that CssIV-induced negative shift lasts longer than Cn2-induced shift. Consequently, as shown by the frequency-dependent accumulation illustrated in Fig. 3, CssIV could produce action potential depolarization block

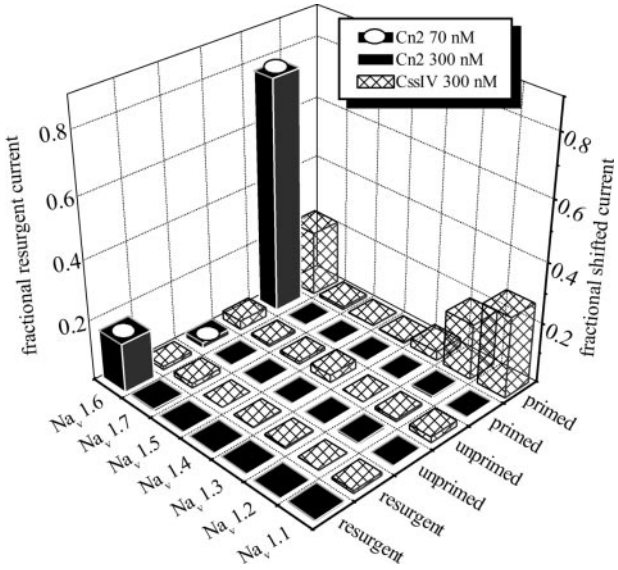

FIGURE 4. **Selectivity of Cn2 and CssIV β-scorpion toxins.** The plot represents the peak fractional resurgent current (at −60 mV; see *left z-axis*) and the fractional peak inward currents (see *right z-axis*) elicited at a membrane potential 10 mV negative to the control threshold for each of the seven different Na^+ channel isoforms. Data are also given under primed and unprimed conditions. The CssIV toxin was used always at 300 nM (*mesh columns*), and the Cn2 toxin (*black columns*) was used at 300 nM in all of the isoforms except in $Na_v1.6$ (*black columns* with *open circle*), where the concentration was 70 nM.

similar to those shown in Fig. 6, also in neurons firing at very low rates.

Purkinje Cells from Cerebellar Tissue Slices Constitutively Express an Intrinsic Resurgent Sodium Current and Cn2 Enhances a Toxin-induced Resurgent Component—Since Cn2 toxin induces a resurgent sodium current in mammalian HEK293 cells expressing Nav1.6 sodium channels that normally do not produce resurgent current, we questioned whether a similar effect could be obtained in a native neuron that already possesses a resurgent sodium current (10). Using the same protocol as that shown in Fig. 2*E*, we studied tissue slices containing cerebellar Purkinje cells in which a resurgent current mainly linked to Nav1.6 channels has been extensively characterized. We found that it evoked a resurgent current (Fig. 5*A*) having the same properties (Fig. 5*C*, *open circles*, $n = 6$) as those shown by Raman and Bean in acutely isolated Purkinje cells (10). This shows for the first time that the resurgent current is also present in the relatively intact Purkinje cells found in tissue slices that have not undergone dissociation, a procedure that implies the loss of almost all dendrites and axonal branches except a short stump. The application of low Cn2 concentrations (35–40 nM) led to a 4-fold increase in the peak amplitude of the resurgent current (Fig. 5*B*) and shifted its voltage dependence by about 30 mV toward more negative potentials, so that the largest current was attained at −60 mV (Fig. 5*C*, *open squares*, $n = 6$). At even more hyperpolarized voltages (−70 or −80 mV), the amplitude of the Cn2-induced resurgent current was still more than twice that of the highest value observed without the toxin. The maximum percentage availability of channels producing the resurgent current was 2.2 ± 0.4% in the control (at −30 mV) and 9.4 ± 2.0% with Cn2 (at −60 mV). During wash-in of the Cn2 toxin, the resurgent current was still unaffected after 1 min and exhibited the largest size at −35 mV.

At 2 min, the physiological resurgent current at −30 mV was unchanged, whereas a larger resurgent current appeared at more negative potentials, demonstrating the largest amplitude at −60 mV. From the third to the fifth minute of Cn2 application, the amplitude of this latter resurgent current increased more than 5-fold, in line with a gradual diffusion of Cn2 inside the tissue (data not shown). The largest amplitude occurred within 5 min of Cn2 application. The sudden appearance of a resurgent current at more negative potentials while the physiological resurgent was unchanged, suggests that, also in Purkinje cells, Cn2 does not simply modify an existing current but induces a novel resurgent current in a different voltage domain.

We then asked whether Cn2 potently blocks the sodium currents of Purkinje cells as it does with those of HEK $Na_v1.6$ cells. We discovered that Cn2 did not block the current with or without the depolarizing prepulse (Fig. 5, *D* and *E*). Fig. 5*F* shows an *I*-V plot of the normalized sodium currents from five Purkinje cells obtained without toxin or prepulse. Peak amplitude occurred at −20 mV, its size neither affected by the toxin nor the prepulse. The effect of Cn2 on sodium currents following a prepulse was a marked leftward shift of the activation threshold, evoking consistent sodium currents at voltages more negative than −60 mV (Fig. 5, *D* and *E*). The normalized conductance plot (Fig. 5*G*) shows that the effect of Cn2 on Purkinje neurons was similar to that obtained using the same dose in $Na_v1.6$-expressing cells (Fig. 1*C*).

In sum, the effect of Cn2 in Purkinje cells substantially confirms the data observed in $Na_v1.6$ α-subunit-expressing cells, with one exception, the huge blocking effect in the latter cells that is absent in Purkinje cells.

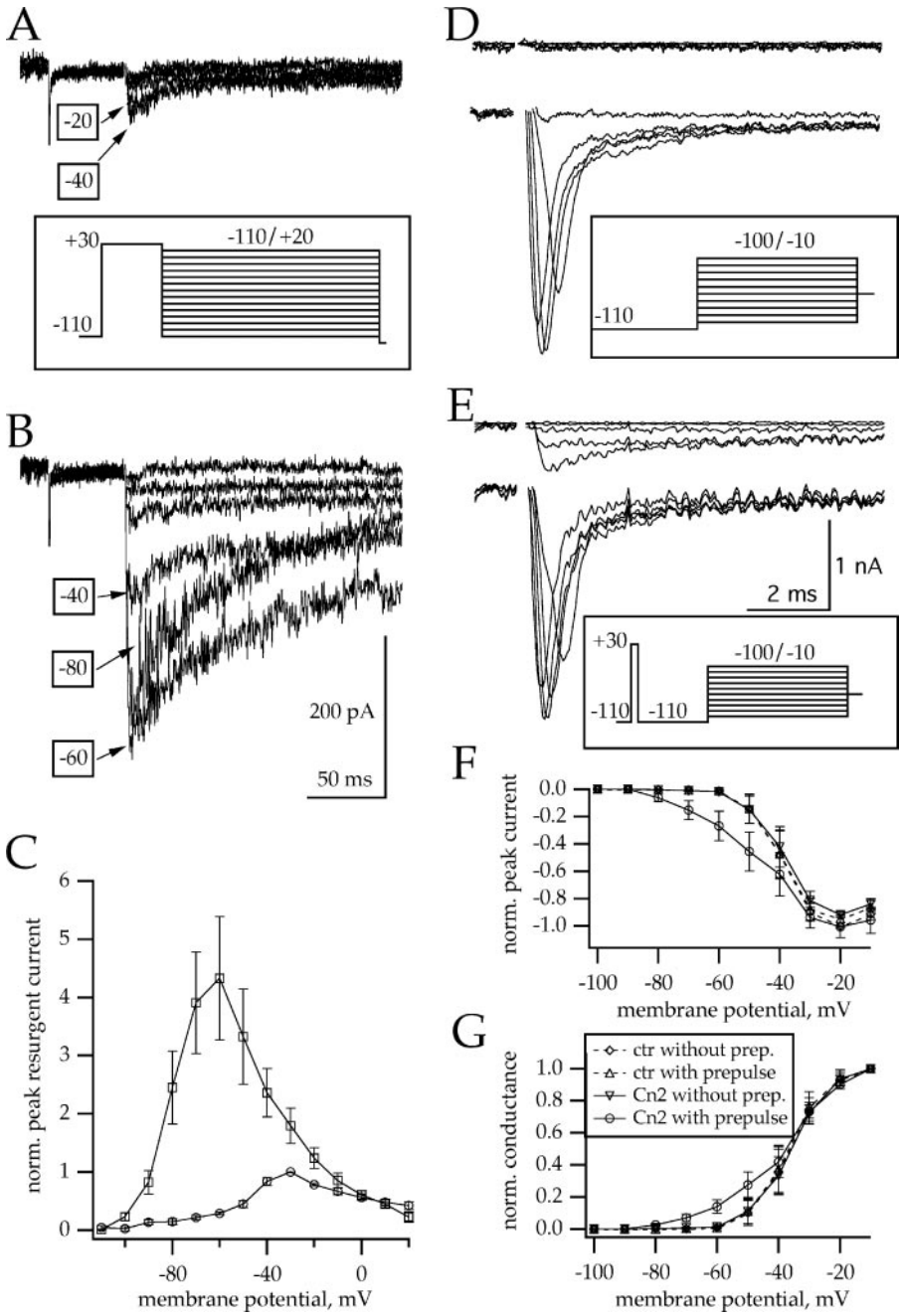

FIGURE 5. **Effects of Cn2 toxin on Purkinje cells in cerebellar slices.** *A* and *B*, resurgent Na^+ currents evoked by voltage steps from +30 mV to different voltages, as indicated in the protocol (*inset*). For clarity, only traces at −80, −60, −40, −20, 0, and +20 mV are shown. *A*, control; *B*, Cn2 (40 nM). Note that in *A*, the largest resurgent current is at −40 mV, whereas in *B*, it is at −60 mV. *Calibration bars* shown in *B* also apply to *A*. *C*, voltage dependence of the peak amplitude of the resurgent current evoked as shown in *A* and *B*. Resurgent current values have been normalized with the amplitude of the control at −30 mV ($n = 6$). *Circles*, control; *squares*, Cn2. Note the leftward shift of 30 mV of the maximal amplitude. *D* and *E*, sodium currents evoked in Purkinje cells by depolarizing steps during application of Cn2 toxin (voltage protocols are shown in the *insets*). *Upper traces*, steps from −100 to −60 mV; *lower traces*, steps from −50 to −10 mV. *D* shows the currents obtained without a priming prepulse. Sodium currents without Cn2 toxin either with or without prepulse (not shown) were identical to those shown in *D*. Note that during Cn2 application, currents evoked after a prepulse were already present at very hyperpolarized voltages (*E*, *upper traces*). *F*, current-voltage relationship normalized to the value at −20 mV without toxin ($n = 5$). Note that only in one condition (with Cn2 and with prepulse) are currents different. *Symbols* in *F* have the same meaning as those in *G*. *G*, normalized conductance-voltage relationship ($n = 5$). Each *curve* was normalized to its maximum value, at −10 mV.

Cn2 Induces Depolarization, Firing Acceleration, and Final Block of Excitability in Cerebellar Purkinje Cells—The application of Cn2 during recording of Purkinje cell membrane potential caused a depolarization and induced firing or increased the spontaneous firing rate. Whereas a small depolarizing current evoked action potential firing in control cells (Fig. 6*A*, *left*), the same magnitude of current increased the spontaneous firing

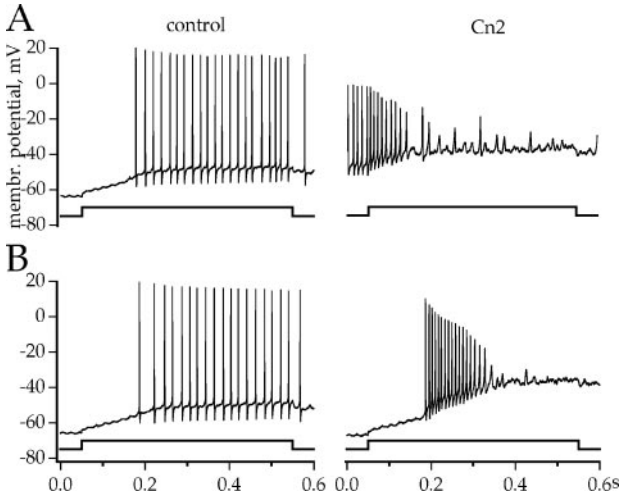

FIGURE 6. **Effects of Cn2 toxin on action potential firing in Purkinje cells in cerebellar slices.** *A*, spontaneous and evoked firing before (control) and after application of Cn2 (35 nM). *B*, Purkinje cell firing evoked from an initial membrane potential of −65 mV, kept by a continuous injection of hyperpolarizing current. Note that in Cn2, the depolarizing phase and the first action potential are not significantly affected, whereas the firing frequency is higher and firing is blocked in less than 200 ms.

rate in Cn2-treated cells, causing inactivation block of the discharge (Fig. 6*A*, *right*). To gain insight into the action of Cn2 on evoked firing while excluding effects on other parameters like spontaneous firing, we maintained the cell at slightly hyperpolarized conditions (−65 mV), thus abolishing spontaneous firing. In these conditions, the injection of a small depolarizing current evoked regular firing in the control (Fig. 6*B*, *left*), whereas in the presence of Cn2, the rate of depolarization and the first action potential were only slightly affected (action potential amplitude from threshold to the peak: control, 62.0 ± 3.8 mV; Cn2, 59.4 ± 3.5 mV; $n = 7$, not significant; action potential rising phase peak velocity: control, 323.3 ± 34.8 V/s; Cn2, 258.1 ± 24.3 V/s; $n = 7$; $p < 0.05$). The trace for Cn2 began to diverge from the control immediately after the end of the first spike, in accordance with the development of a resurgent sodium current. Thus, the first interspike interval was significantly shorter (control 9.4 ± 1.9 ms; Cn2 7.7 ± 1.8 ms; $n = 7$; $p < 0.05$), indicating firing acceleration, and the second action potential was significantly smaller (control, 43.2 ± 3.0 mV; Cn2, 32.1 ± 3.2 mV; $n = 7$; $p < 0.01$) and slower (peak velocity control, 174.4 ± 19.4 V/s; Cn2, 99.3 ± 10.6 V/s; $n = 7$; $p < 0.01$). Subsequent spikes were gradually more severely affected, so that inactivation block occurred (Fig. 6, *B* and *C*). When stimulation ceased, the cells recovered from the inactivation block either spontaneously or following injection of a stronger hyperpolarizing current. With injection of depolarizing current, the cell discharge showed a gradual frequency adaptation, until the firing ceased completely. In these conditions, the duration of the evoked discharge was significantly reduced following Cn2 application (to 60.5 ± 7.6% relative to the control; $n = 7$; Student's paired *t* test; $p < 0.01$), corresponding to an earlier inactivation block of evoked discharge. This behavior indicates that Cn2 is likely to produce inactivation block in cells subjected to a tonic excitatory drive.

DISCUSSION

Most models of ion channel gating (2) describe the depolarization-induced inactivation process as an interaction involving both outward movements of S4 charged segments (opening of the channel) and the inactivation particle that links III and IV domains from the intracellular side. Specifically, the binding of the inactivation particle immobilizes S4 segments of domains III and IV (but not IS4 and IIS4) in the outward position. Repolarization-induced recovery from inactivation starts with the detachment of the inactivation particle from the S4 segments, which regain their final resting position. Since this detachment is a slow process and repositioning of IS4 and IIS4 is a fast process, no ion current (resurgent current) is seen immediately after repolarization, because the channels are virtually closed. Indeed, this observation fits the conventional mechanism of sodium channel inactivation, from which recovery is thought to proceed through closed states (33).

The first insightful description of the biophysical effects of scorpion toxins, such as those described herein, was obtained with the venom of *C. sculpturatus* in the frog node of Ranvier in 1975 (for a review, see Ref. 25). Molecular biology and tissue expression of Na^+ ion channels on one hand and purification, sequencing, and structure-function studies of toxin peptides on the other hand, have progressed in such a way that in recent years only comparative studies of the action of very similar and completely characterized peptides on wild type (20) or on mutated isoforms of the same channel provide the means to answer highly specific questions concerning toxin-channel interaction.

Indeed, site-directed mutagenesis studies using the $rNa_v1.2$ channel allowed Catterall and co-workers (4) to study and interpret the effects of the scorpion *C. suffusus suffusus* toxin CssIV as a negative shift of the activation. When repolarization was applied to inactivated CssIV-primed channels, as Cahalan did in the *C. sculpturatus* envenomed frog node, no currents (resurgent) were observed in the negative membrane potential region, where the channels were induced to open by the toxin itself. On the contrary, toxin-induced tail currents were observed to increase in a region much more negative than −80 mV, where channels, in CssIV, were not able to open. These data were interpreted as currents through channels that were no longer inactivated but rather were deactivating much more slowly by the trapping mechanism (6).

Here, we describe the unique properties of a β-scorpion toxin, Cn2, capable of simultaneously shifting the activation curve and producing resurgent currents in only one target among the seven TTX-sensitive Na^+ isoforms, the $Na_v1.6$ channel. This alternative approach for producing resurgent currents is structurally very different from that extensively studied in Purkinje cells (12). However, both should, in principle, produce resurgent currents with different properties in the cerebellar cell itself as documented here. Indeed, our comparative data shown in Fig. 4 suggest that the peptide CssIV is unable to produce resurgent currents in any of the tested isoforms, thus substantiating Catteral's data (6).

In the presence of a β-toxin, such as Cn2, the IIS4 segment is forced into an unusual position by the peptide as a consequence

of the sensor-trapping mechanism (4). Thus, we hypothesize that the channel-closing process could be delayed as previously suggested (6), rather than accelerated. As a consequence, the inactivation particle could detach simultaneously with channel deactivation, providing a means for detecting open channels (resurgent current) in a region more positive than −80 mV. This implies that Cn2 should bind to at least one other channel region besides the trapping region.

Although the technique of priming Na^+ channels during scorpion toxin perfusion is very old (7), there are no studies concerning the possibility of measuring the transient duration of the negative shift in the voltage-dependent activation. During our studies, as shown in Fig. 2, *A* and *B*, we discovered that such a time course does exist for primed channels. Thus, the model of the voltage sensor-trapping mechanism and the concept of an unconventional resurgent current could be linked together by the Cn2 toxin, resulting in two facets of the same observation: the binding of a toxin peptide to specific amino acid residues of the $Na_v1.6$ channel.

Collectively, our results provide a description of an $hNa_v1.6$ Na^+ channel that can be switched for a short time (200–300 ms) through voltage priming in the presence of Cn2, into an ion channel capable of opening at normally prohibitive hyperpolarized voltages. Interestingly, this ability is permitted either from closed states in a conventional manner (also for CssIV), or from inactivated states (only for Cn2) through an unconventional recovery process characterized by time constants different from those observed in normal channels but able to generate a resurgent current.

Whereas it is known that $Na_v1.6$ transcripts and channels are expressed throughout the developmental process in adult brain, nodes of Ranvier, unmyelinated axons, cell bodies, dendrites, and presynaptic terminals (31, 32, 34, 35) and that up to five different β-subunits can modify the functioning of the different α-subunits (see Ref. 23), it remains to be determined if putative Cn2-like toxins from other scorpions are sufficiently selective to attack other isoforms or if different combinations of α- and β-subunits can alter the bindings of these peptides.

Amino Acid Sequence of the IIS3-S4 Loop among the Other TTX-sensitive Na^+ Channel Isoforms and Putative Origin of Toxin-induced Differences Observed in HEK Cells in Mice Purkinje Cells—It is known that the G845N mutation (gray box in second row of Table 1) of the $rNa_v1.2$ channel considerably decreases the affinity of CssIV for its receptor site as well as its electrophysiological effects (6). Further investigations have shown that the two outermost positive charges Arg^{850} and Arg^{853} (gray boxes in Table 1) are crucial and greatly change the action of CssIV (6, 36). The region of the S4 segment investigated by Cestèle *et al.* (6) is almost identical in all isoforms. Thus, it is unlikely that the $Na_v1.6$ selectivity for Cn2 is related either to this part of the protein or simply to the glycine 845, also present in all other isoforms (except $Na_v1.5$). In the S3-S4 extracellular loop amino acid sequence NVEGL (see Table 1), the polar asparagine (conserved in $Na_v1.1$, −1.2, −1.3, and −1.4) is substituted by a charged aspartate in $Na_v1.6$ and $Na_v1.7$ channels. However, since no resurgent currents were seen in $rNa_v1.7$, we are not convinced that this amino acid substitution is critical.

TABLE 1

Amino acid sequence of $xNa_v1.x$ channel alignment in domain II of the region between the end of the segment S3 and the beginning of segment S4

From top to bottom the following accession numbers have been used: P04775, P35498, Q99250, Q9NY46, P35499, Q14524, Q9UQD0, Q9WTU3, and O08562. The amino acids are indicated only for $Na_v1.1$, and the changes are indicated in light gray or black background for conservative or nonconservative substitutions, respectively. The gray boxes in the $hNa_v1.2$ row show the positions of the amino acids altered by Cestèle *et al.* (6).

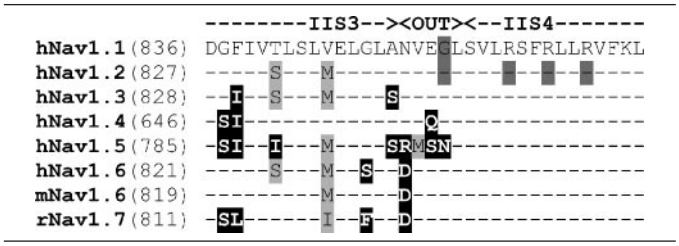

Another unexplained effect concerns the blocking action of Cn2 on unprimed Na^+ currents observed in the α-subunit-expressing cells as compared with Purkinje cells, in which Cn2 fails to block current. A possible explanation could originate once again from a putative β-subunit specificity, because in the HEK cells used for stable expression of $Na_v1.6$, it is known (37) that only the β1A subunit is intrinsically expressed and not the β4, critical for generating the intrinsic resurgent current (12). These unanswered questions are the basis for future studies.

Structural Differences between Cn2 and CssIV—There are structural differences in 11 of 66 positions (*i.e.* the two toxins have 83% identical amino acids in equivalent positions) (see Fig. 7). Some of these differences, such as Y14F (Y in Cn2, F in CssIV), L17F, K30R, and I56V, are considered conservative substitutions, because they maintain the hydrophobic or charge character of the amino acids. Substitutions such as A37S and A45G are more important but distant from D7N, K8S, and N9Y on the N-terminal side and R64T and S*66N of the C-terminal region of both molecules (the S* means that the last serine is amidated in Cn2). There are no differences between Cn2 and CssIV (see *f* in the *last row* of Fig. 7) in any of the positions recently shown by Cohen *et al.* (38) to be important for the binding of CssIV to channel site 4; all of them are identical, including position E15E, which, when mutated to E15R in the recombinant CssIV toxin, made a difference because it abolished the left shift of the voltage-dependent current assayed in the channel (39). This suggests that the significant differences in the most N- and C-terminal sections of Cn2 indicate the site responsible for the resurgent current mechanism found in Cn2 but not in CssIV. It is worth noting that the cysteines in positions Cys^{12} and Cys^{65} join both the N- and C-terminal segments of Cn2 via a disulfide bridge. This region has been shown to be important for neutralizing the toxic effect of Cn2 in mice by means of BCF2, a neutralizing mouse antibody that recognizes Cn2 (14, 40) and synthetic peptides corresponding to these segments of the primary Cn2 structure (39). Furthermore, NMR three-dimensional structure determinations have shown that the same Cn2 segments are spatially packed together (13, 41). The segment that mainly comprises the loop in positions Asp^7–Cys^{11} forms the central part of the epitope, a region that differs significantly between the primary structures of Cn2 and CssIV, as discussed above

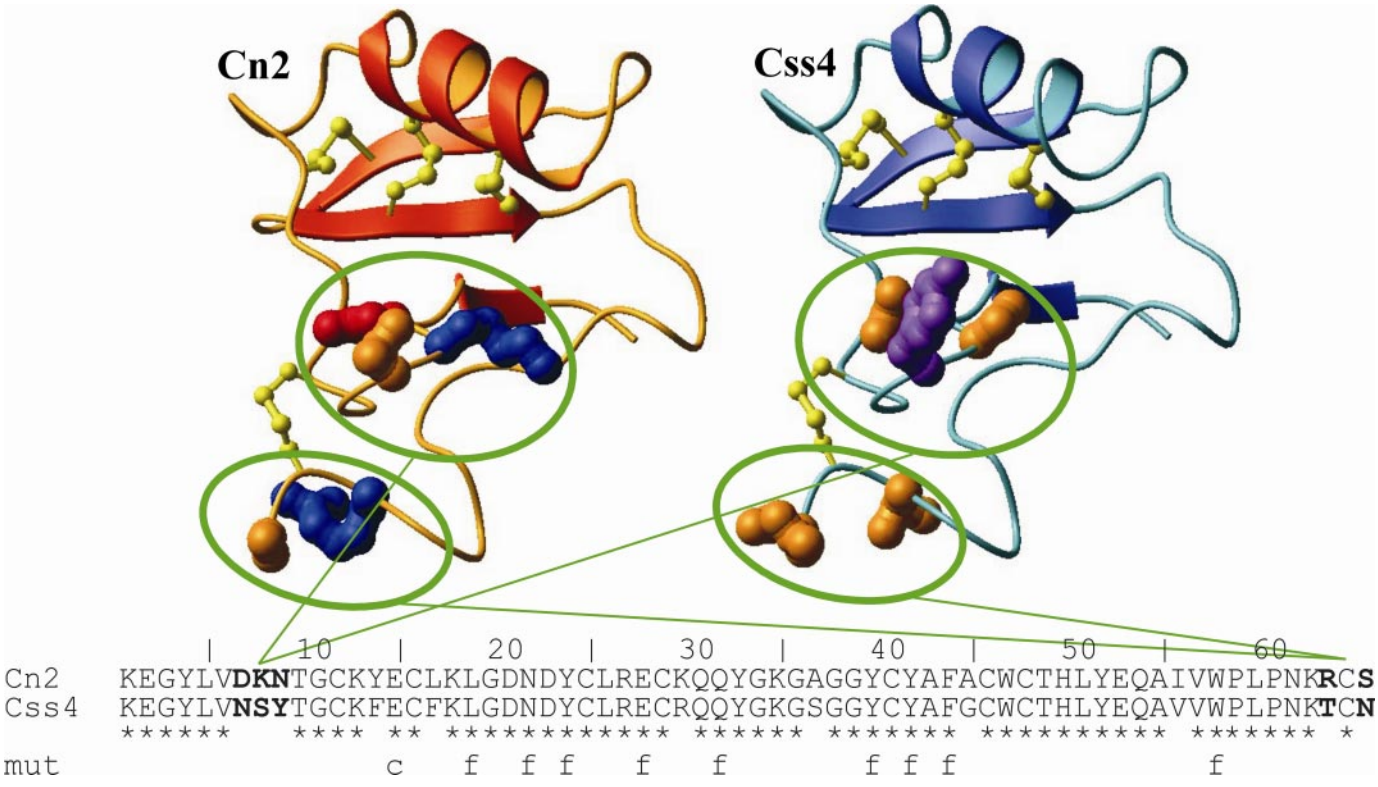

FIGURE 7. **Structural differences between Cn2 and CssIV.** The three-dimensional structure of Cn2 (*left*, *orange colors*) and modeled CssIV (*right*, *blue colors*) shows clusters of amino acid differences (*green circles*). The *bottom lines* show the alignment of both toxins highlighting the residues important for CssIV action on rNav1.2 (in the mutant (*mut.*) *row*, *f* marks residues important for function, and *c* marks a conserved residue on β-scorpion toxins important for Na^+ channel modulation but not for membrane binding (38).

and shown in Fig. 7. All of the currently available data, therefore, suggest that it is this Cn2 surface that makes the functional difference when interacting with the $Na_v1.6$ channel; both Cn2 and CssIV cause a leftward shift of the current, but only Cn2 produces a resurgent current.

Modulation of $Na_v1.6$ Currents and Parkinson Disease—The progressive degeneration of dopaminergic neurons in Parkinson disease leads to gradual motor impairment due to complex dysfunctional rearrangements in neural circuits. It is known that pathological self-sustaining hyperactivity occurs in the two major output regions of the striatum, the subthalamic nucleus and the internal globus pallidus (42). It is worth noting that functional interference with the deranged loop activity of patients by means of high frequency electrical stimulation of these nuclei has major therapeutic value (43). More recently, it has also been demonstrated that motor cortex stimulation alleviates a primate model of the disease (44).

It has been shown (45) that such stimulations block the Na^+ voltage-gated currents known to be mainly of the $Na_v1.6$ type. Furthermore, a recent comparison of the same neurons and Purkinje neurons (46, 47) suggests that slow inactivation or other putative sodium currents may contribute to the intriguing roles of resurgent and persistent currents. Since our study shows that Cn2 not only has sharp channel selectivity and binding stability for the $Na_v1.6$ isoform but also blocks firing in Purkinje neurons at appropriate concentrations, we propose using Cn2 as a leading compound for the study of Parkinson disease.

Acknowledgments—We thank Dr. Ricardo Rodríguez de la Vega for critically reading the manuscript and Dr. J. J. Clare for permitting the use of GlaxoSmithKline $Na_v1.x$ cell clones; we warmly thank Dr. Gerardo Corzo for the toxin CssIV purification; we also thank Dr. F. Gullo for help in preparing the chromaffin cells, G. Mostacciuolo for making technical improvements, and Dr. Deyanira Fuentes Silva for the sodium channel alignments.

REFERENCES

1. Catterall, W. A. (2000) *Neuron* **26,** 13–25
2. Cha, A., Ruben, P. C., George, A. L., Jr., Fujimoto, E., and Bezanilla, F. (1999) *Neuron* **22,** 73–87
3. Rogers, J. C., Qu, Y., Tanada, T. N., Scheuer, T., and Catterall, W. A. (1996) *J. Biol. Chem.* **271,** 15950–15962
4. Cestèle, S., Qu, Y., Rogers, J. C., Rochat, H., Scheuer, T., and Catterall, W. A. (1998) *Neuron* **21,** 919–931
5. Cestèle, S., and Catteral, W. A. (2000) *Biochimie* (*Paris*) **82,** 883–892
6. Cestèle, S., Scheuer, T., Mantegazza, M., Rochat, H., and Catterall, W. A. (2001) *J. Gen. Physiol.* **118,** 291–301
7. Cahalan, M. D. (1975) *J. Physiol.* **244,** 511–513
8. Meves, H., Rubly, N., and Watt, D. D. (1982) *Pfluegers. Arch.* **393,** 56–62
9. Wang, G. K., and Strichartz, G. R. (1983) *Mol. Pharmacol.* **23,** 519–533
10. Raman, I. M., and Bean, B. P. (1997) *J. Neurosci.* **17,** 4517–4526
11. Raman, I. M., Sprunger, L. K., Meisler, M. H., and Bean, B. P. (1997) *Neuron* **19,** 881–891
12. Grieco, T. M., Malhotra J. D., Chen C., Isom L. L., and Raman, I. M. (2005) *Neuron* **25,** 233–244
13. Pintar, A., Possani, L. D., and Delepierre, M. (1999) *J. Mol. Biol.* **287,** 359–367
14. Zamudio, F., Saavedra, R., Martin, B. M., Gurrola-Briones, G., Herion, P.,

and Possani, L. D. (1992) *Eur. J. Biochem.* **204,** 281–292
15. Rochat, H., Darbon, H., Jover, E., Martin, M. F., Bablito, J., and Couraud, F. (1984) *J. Physiol.* (*Paris*) **79,** 334–337
16. Martin, M. F., Garcia y Perez, L. G., El Ayeb, M., Kopeyan, C., Bechis, G., Jover, E., and Rochat, H. (1987) *J. Biol. Chem.* **262,** 4452–4459
17. Schwede, T., Kopp, J., Guex, N., and Peitsch, M. C. (2003) *Nucleic Acids Res.* **31,** 3381–3385
18. Hooft, R. W. W., Vriend, G., Sander, C., and Abola, E. E. (1996) *Nature* **381,** 272–272
19. Koradi, R., Billeter, M., and Wüthrich, K. (1996) *J. Mol. Graphics* **14,** 51–55
20. Oliveira, J. S., Redaelli, E., Zaharenko, A. J., Restano Cassulini, R., Konno, K., Pimenta, D. C., Freitas, J. C., Clare, J. J., and Wanke, E. (2004) *J. Biol. Chem.* **279,** 33323–33335
21. Gullo, F., Ales, E., Rosati, B., Lecchi, M., Masi, A., Guasti, L., Cano-Abad, M. F., Arcangeli, A., Lopez, M. G., and Wanke, E. (2003) *FASEB J.* **17,** 330–332
22. Klugbauer, N., Lacinova, L., Flokerzi, V., and Hofmann, F. (1995) *EMBO J.* **14,** 1084–1090
23. Goldin, A. L. (2001) *Annu. Rev. Physiol.* **63,** 871–894
24. Burbidge, S. A., Dale, T. J., Powell, A. J., Whitaker, W. R. J., Xie, X. M., Romanos, M. A., and Clare, J. J. (2002) *Mol. Brain Res.* **103,** 80–90
25. Hille, B. (2001) *Ionic channels of Excitable Membranes*, pp. 635–640, Sinauer Associates, Inc., Sunderland, MA
26. Llinas, R., and Sugimori, M. (1980) *J. Physiol.* (*Lond.*) **305,** 171–195
27. Sacco, T., and Tempia, F. (2002) *J. Physiol.* (*Lond.*) **543,** 505–520
28. Smith, M. R., Smith, R. D., Plummer, N. W., Meisler, M. H., and Goldin, A. L. (1998) *J. Neurosci.* **18,** 6093–6102
29. Herzog, R. I., Cummins T. R., Ghassemi, F., Dib-Hajj, S. D., and Waxman, S. G. (2003) *J. Physiol.* **551,** 741–750
30. Raman, I. M., and Bean, B. P. (2001) *Biophys. J.* **80,** 729–737
31. Caldwell, J. H., Schaller, K. L., Lasher, R. S., Peles, E., and Levinson, S. R. (2000) *Proc. Natl. Acad. Sci. U. S. A.* **97,** 5616–5620
32. Schaller, K. L., and Caldwell, J. H. (2000) *J. Comp. Neurol.* **420,** 84–97
33. Kuo, C. C., and Bean, B. P. (1994) *Neuron* **12,** 819–829
34. Boiko, T., Rasband, M. N., Levinson, S. R., Caldwell, J. H., Mandel, G., Trimmer, J. S., and Matthews, G. (2001) *Neuron* **30,** 91–104
35. Krzemien, D. M., Schaller, K. L., Levinson, S. R., and Caldwell, J. H. (2000) *J. Comp. Neurol.* **420,** 70–83
36. Mantegazza, M., and Cestèle, S. (2005) *J. Physiol.* **568,** 13–30
37. Moran, O., Nizzari, M., and Conti, F. (2000) *FEBS Lett.* **473,** 132–134
38. Cohen, L., Karbat, I., Gilles, N., Ilan, N., Benveniste, M., Gordon, D., and Gurevitz, M. (2005) *J. Biol. Chem.* **280,** 5045–5053
39. Calderón-Aranda, E. S., Selisko, B., York, E. J., Gurrola, G. B., Stewart, J. M., and Possani, L. D. (1999) *Eur. J. Biochem.* **264,** 746–755
40. Licea, A. F., Becerril, B., and Possani, L. D. (1996) *Toxicon* **34,** 843–847
41. Selisko, B., Licea, A. F., Becerril, B., Zamudio, F., Possani, L. D., and Horjales, E. (1999) *Proteins* **37,** 130–143
42. DeLong, M. R. (1990) *Trends Neurosci.* **13,** 281–285
43. Krack, P., Pollak, P., Limousin, P., Hofmann, D., Xie, J., Benazzouz, A., and Benabid, A. L. (1998) *Brain* **121,** 451–457
44. Drouot, X., Oshino, S., Jarraya, B., Besret, L., Kishima, H., Remy, P., Dauguet, J., Lefaucheur, J. P., Dollè, F., Condè, F., Bottlaender, M., Peschanski, M., Keravel, Y., Hantraye, P., and Palfi, S. (2004) *Neuron* **44,** 769–778
45. Beurrier, C., Bioulac, B., Audin, J., and Hammond, C. (2001) *J. Neurophysiol.* **85,** 1351–1356
46. Do, M. T., and Bean, B. P. (2003) *Neuron* **39,** 109–120
47. Do, M. T., and Bean, B. P. (2004) *J. Neurophysiol.* **92,** 726–733

Resurgent Current and Voltage Sensor Trapping Enhanced Activation by a β -Scorpion Toxin Solely in $Na_V1.6$ Channel: SIGNIFICANCE IN MICE PURKINJE NEURONS

Emanuele Schiavon, Tiziana Sacco, Rita Restano Cassulini, Georgina Gurrola, Filippo Tempia, Lourival D. Possani and Enzo Wanke

J. Biol. Chem. 2006, 281:20326-20337.
doi: 10.1074/jbc.M600565200 originally published online May 15, 2006
